Article

A Two-Season Impact Study of Radiative Forced Tropospheric Response to Stratospheric Initial Conditions Inferred From Satellite Radiance Assimilation

Min Shao [1] **, Yansong Bao** [2,3]**, George P. Petropoulos** [4,5] **and Hongfang Zhang** [6,*]

1   Atmospheric & Planetary Science, Hampton University, Hampton, VA 23669, USA; mshao@masonlive.gmu.edu
2   Collaborative Innovation Center on Forecast and Evaluation of Meteorological Disasters, CMA Key Laboratory for Aerosol-Cloud-Precipitation, Nanjing University of Information Science & Technology, Nanjing 210044, China; ysbao@nuist.edu.cn
3   School of Atmospheric Physics, Nanjing University of Information Science & Technology, Nanjing 210044, China
4   School of Mineral Resources Engineering, Technical University of Crete, Kounoupidiana Campus, 73100 Crete, Greece; petropoulos.george@gmail.com or gpetropoulos@isc.tuc.gr
5   Department of Soil & Water Resources, Institute of Industrial & Forage Crops, Ellenic Agricultural Organization (HAO) "Demeter", 14335 Larisa, Greece
6   Shaanxi Meteorological Service Centre, Xi'an 710014, China
*   Correspondence: hongfangji@sohu.com; Tel.: +86-2821037682

check for updates

Abstract: This study investigated the impacts of stratospheric temperatures and their variations on tropospheric short-term weather forecasting using the Advanced Research Weather Research and Forecasting (WRF-ARW) system with real satellite data assimilation. Satellite-borne microwave stratospheric temperature measurements up to 1 mb, from the Advanced Microwave Sounding Unit-A (AMSU-A), the Advanced Technology Microwave Sounder (ATMS), and the Special Sensor microwave Imager/Sounder (SSMI/S), were assimilated into the WRF model over the continental U.S. during winter and summer 2015 using the community Gridpoint Statistical Interpolation (GSI) system. Adjusted stratospheric temperature related to upper stratospheric ozone absorption of short-wave (SW) radiation further lead to vibration in downward SW radiation in winter predictions and overall reduced with a maximum of 5.5% reduction of downward SW radiation in summer predictions. Stratospheric signals in winter need 48- to 72-h to propagate to the lower troposphere while near-instant tropospheric response to the stratospheric initial conditions are observed in summer predictions. A schematic plot illustrated the physical processes of the coupled stratosphere and troposphere related to radiative processes. Our results suggest that the inclusion of the entire stratosphere and better representation of the upper stratosphere are important in regional NWP systems in short-term forecasts.

Keywords: data assimilation; coupled stratosphere-troposphere; WRF; microwave instruments; earth observation

1. Introduction

It is well-established that stratospheric circulation systems and events are strongly influenced by tropospheric eddy perturbations [1–5]. In recent decades, evidence has also indicated that stratospheric perturbations can affect tropospheric systems [6–11]. Simplified climate models and atmospheric

general circulation models have already been used to study the mechanisms of the coupled stratosphere and troposphere [12–15]. These mechanisms include the downward propagation of stratospheric perturbations, such as the Arctic Oscillation [16], and stratospheric thermal forcing such as polar stratospheric cooling and sudden stratospheric warming (SSW) [15,17,18], as well as chemical exchanges between the stratosphere and troposphere [19].

To our knowledge, the impacts of the stratosphere on the troposphere have not yet been comprehensively studied in weather forecasting models. This is due to the timescale on which stratospheric events affect tropospheric events is usually the seasonal scale. It has been suggested in the literature that inclusion of stratospheric forcing can bring improved prediction skill for tropospheric weather forecasting [20,21]. Most models that represent the stratosphere in regional numerical weather prediction (NWP) systems usually consider only very bottom part of the stratosphere (etc. the top model boundary is set at 100 mb).

However, stratospheric circulations (e.g., the Brewer–Dobson Circulation, BDC) and events (e.g., SSWs) usually have a broader spread in terms of their vertical extent. Also, the radiation balance in the tropical tropopause layer (TTL) is strongly bounded with the water vapor content and radiative heating [22]. Therefore, inclusion of the entire stratosphere and a better representation of the stratosphere in regional NWP systems will likely improve our understanding of the coupled stratosphere–troposphere in regional weather predictions. Stratospheric perturbations usually take one to three months to affect the troposphere [13,14,20] whereas regional weather prediction models often have a synoptic-scale response time (days).

Accuracy of regional model predictions is dependent on the quality of the initial conditions. Data assimilation aims to generate initial conditions with better quality than otherwise possible, improving the representation of the stratosphere in regional NWP systems [23]. Satellite-borne instruments are generally used to make stratospheric observations, where the observational weighting function indicates the altitude range of over which the measurements are useful [24].

Utilization of infrared and microwave measurements generally have different and distinct impacts on tropospheric weather prediction models [25]. As noted by Zou et al. (2013) [26], more valuable information within and below clouds can be obtained when using microwave radiance technologies. Microwave radiation can penetrate non-precipitation clouds as well as carrying atmospheric humidity information within the cloud, as compared to infrared humidity sensors which do not give this information. In NWP systems, Cucuruul and Anthes (2014) [25] evaluated satellite microwave measurements of the stratosphere. Authors found that they can lead to larger impacts than infrared measurements when assimilated separately in the global operational forecast model in NCEP. Also, recently, Shao (2017) [27] found that microwave measurements lead to better improvements in both tropopause and stratospheric analysis and predictions than infrared measurements when each are assimilated separately in regional model WRF.

In this study the regional model top boundary is raised to 1 mb in order to include the entire stratosphere and demonstrate the importance of assimilating stratospheric observations in a regional NWP system by comparing winter and summer short-term predictions with adjusted stratospheric initial conditions through assimilation of microwave stratospheric measurements from AMSU-A, ATMS, and SSMI/S. The paper is structured as follows: the data assimilation scheme is described in Section 2; the data usage and model configurations are made available in Section 3; the analysis and predictions are covered in Sections 4 and 5, respectively and finally a summary and conclusion are made available in Section 6.

2. Assimilation Scheme

The GSI 3D-Var-based Ensemble-Variational Hybrid Data Assimilation scheme is used in this study [28–30]. This scheme uses the background error covariance matrix, which is completely static or only slightly coupled to the dynamics of the forecast, and at the same time involves the fully flow-dependent background error covariance estimated from a set of ensembles of short-range

forecasts with the WRF forecast model [29]. The cost function for this hybrid data assimilation can be described as follows:

$$J(\boldsymbol{x}) = \frac{1}{2}\beta_1(\boldsymbol{x} - \boldsymbol{x}_b)^T \boldsymbol{B}_f^{-1}(\boldsymbol{x} - \boldsymbol{x}_b) + \frac{1}{2}\beta_2(\boldsymbol{x} - \boldsymbol{x}_b)^T \boldsymbol{B}_{ens}^{-1}(\boldsymbol{x} - \boldsymbol{x}_b) + \frac{1}{2}\big[\boldsymbol{y}_o - H(\boldsymbol{x})\big]^T \boldsymbol{R}^{-1}\big[\boldsymbol{y}_o - H(\boldsymbol{x})\big] \quad (1)$$

where $\boldsymbol{x}$, $\boldsymbol{x}_b$ and $\boldsymbol{y}_o$ are vectors of the analysis, background fields and observations, respectively. $\boldsymbol{B}_f$ and $\boldsymbol{B}_{ens}$ are the model static background error covariance and background error covariance estimated from a set of ensemble forecasts, respectively. $\boldsymbol{R}$ is the observational error covariance and H is the observation forward operator which converts the model state to the observational state. β_1 and β_2 are two factors whose inversions define the weights placed on the static covariance and the ensemble covariance where these two factors satisfy the relation $\frac{1}{\beta_1} + \frac{1}{\beta_2} = 1$.

Satellite measurements used in this study are directly assimilated into the system. For this purpose, the Community Radiative Transfer Model (CRTM) developed by the Joint Center for Satellite Data Assimilation (JCSDA) is employed in the data assimilation system and serves as the forward observation operator for radiance measurements [31]. CRTM calculates the absorption of atmospheric gases, scattering, and absorption by both clouds and aerosols, and surface emissivity and reflectivity, and then solves the radiative transfer problem. Observed radiance data with low reliability due to uncertainties in the formation of the radiative transfer equation or the unknown parameters in the radiative transfer equation are removed through quality-control steps [32]. Cloud contaminated radiance observations are also removed. Satellite radiance data thinning is also applied based on the horizontal resolution of the field of view of each instrument.

3. Data & Model Configuration

Experiments are conducted on the Supercomputer for Satellite Simulation and Data Assimilation Studies (S4) system [33]. The AMSU-A, ATMS and the SSMI/S temperature measurement channels were selected in this study. Stratospheric temperature measurements channels are further refined based on the weighting functions of each channel. In winter, the AMSU-A channels 7 to 14, the ATMS channels 8 to 15, and the SSMI/S channels 5 to 7 and 22 to 24, are selected because their maximum weighting functions are located in the stratosphere and have little impact on the troposphere. In summer, the AMSU-A channels 8 to 14, the ATMS channels 9 to 15, and the same SSMI/S channels in winter, are selected due to the lifted tropopause in summer. The level-1b brightness temperature measured by these channels along with conventional observations over the continental U.S., are assimilated for January (winter) and July (summer) 2015.

The Global Forecast System (GFS) full-atmosphere products with a horizontal resolution of 0.25° by 0.25° and a model top set at 1-mb are used as the initial atmospheric and lateral boundary conditions for the WRF-ARW which uses non-hydrostatic deep momentum equations and is produced by the National Center for Atmospheric Research (NCAR), the Air Force Weather Agency, the National Oceanic and Atmospheric Administration (NOAA), and other governmental agencies and universities. The physic schemes in WRF-ARW are as follows: the New Thompson scheme [34] (Thompson et al., 2008) for microphysics; the RRTMG schemes [35] *(Iacono* et al., *2008)* for both longwave and shortwave radiation; the MYNN surface layer scheme [36] (Nakanishi and Niino 2009) for surface layer; the RUC land surface model [37] (Smirnova et al. 2016) for surface physics; the Mellor-Yamada Nakanishi and Niino Level 2.5 scheme [36] (Nakanishi and Niino 2009) for the planetary boundary layer; and the Grell-Freitas scheme [38] (Grell and Freitas 2014) for the cumulus parameterization.

The horizontal resolution used in this study is 0.1° by 0.1° with one domain covering the whole continental United States (21°N–53°N, 74°W–115°W). Sixty-one vertical levels are specified with 40 of these layers in the stratosphere. The same observation forward operators, satellite bias correction algorithms and quality-control decisions as in the operational 3D-Var system are used [31,39]. The operational global static background error covariance is used. The ensembles used in this study are prepared using the WRF-ARW by adding random perturbations to the initial conditions and making a

6-h forecast. The covariance localization scale (1000 km) is also applied on the ensemble covariance to remove long-range spurious ensemble covariance to remove long-range spurious correlations and increase the effective ensemble size [40]. Due to limited computational resources, forty ensembles were generated for each initial state. Two experiments were conducted for January and July 2015. The first experiment (EXP1) assimilated all the stratospheric temperature measurement channels from AMSU-A, ATMS and SSMI/S. The second experiment (EXP2) is the control experiment with no data assimilation. The differences between EXP1 and EXP2 are then inferred as the atmospheric response of the adjusted stratospheric initials. A 6-h data assimilation cycle is applied with introducing the larger-scale global information from GFS every 5 days to provide better longwave representation [41]. The weights set to the static background error covariance and the ensemble-based background error covariance are 0.2 and 0.8, respectively. Thus, around 120 analyses were obtained during both seasons. One-week predictions were made using the updated initial conditions. Thus, the impacts from the initial conditions can be studied through the comparison of the average state of the analysis and predictions from EXP1 and EXP2.

4. Adjusting the Analysis

The stratospheric temperature analysis differences between EXP1 and EXP2 are plotted in Figure 1. For the winter temperature analysis differences (Figure 1a), a warmer upper stratosphere (5 mb to 1 mb) was obtained by assimilating the microwave stratospheric measurements. The maximum warming region is located between 30°N and 40°N with a value of 2.6 K. In contrast, a cooled lower stratosphere was obtained, especially over the ozone layer (−0.5 K). The adjusted upper stratospheric temperature profile can lead to a more stable stratosphere. In summer (Figure 1b), a warmer upper stratosphere was obtained in the mid-latitudes, while a cooler upper stratosphere with a maximum cooling effect of 1.4 K was obtained over the tropics and extra-tropics.
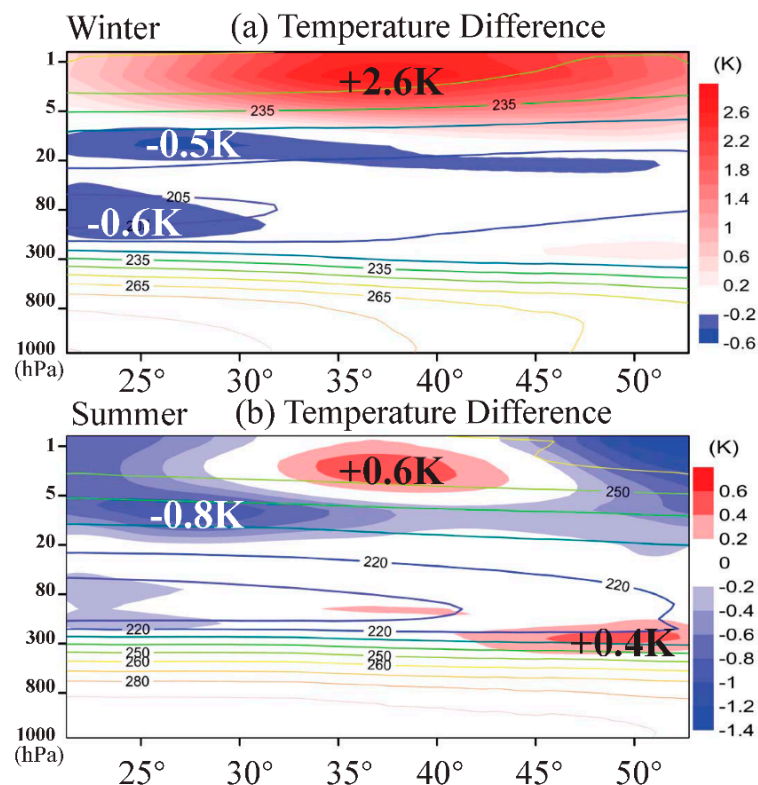

Figure 1. Zonally averaged vertical temperature differences (shaded) between EXP1 and EXP2 over the longitudinal domain of the regional model' during both (**a**): winter and (**b**): summer and the base state (contours).

A relatively unstable stratosphere was obtained in summer compared to winter. The temperature analysis differences in the lower stratosphere are similar to those in winter. Both winter and summer show a cooler stratosphere in the tropics and a warmer lower stratosphere in the extra-tropics. The corresponding temperature adjustments may lead to the adjusted radiative processes related to variations in ozone in the mid and upper stratosphere.

5. Responses in Short-Term Predictions

As discussed in Gerber et al. (2009) [42] and Karpechko et al. (2017) [43], downward propagating major SSW events in the lower stratosphere, have a larger chance of affecting tropospheric weather forecast predictabilities due to their impacts on tropospheric circulation systems. These major SSW events are usually characterized by a more negative Northern Annular mode index and enhanced wave propagation to the stratosphere in the first few forecast days. However, it usually takes one to three months for the propagation to have any significant impact on the troposphere. Also, consistent changes to tropospheric synoptic-scale systems occur in response to the stratospheric initial conditions, starting at 5-day forecast lead times [20]. In this study, a faster response of the tropospheric regional circulations to the assimilated microwave stratospheric temperature measurements was observed. The regional circulations here [e.g., the regional Hadley Cell (HC), Ferrel Cell (FC) and Polar Cell (PC)] differ from the conventional definitions because of the regional study domain. The predicted zonally averaged temperature, downward short-wave (SW) radiation, geopotential height (GPH), and relative humidity (RH) differences (shaded) between EXP1 and EXP2 and the base state from EXP2 (contours) at the 12-h forecast lead time over the longitudinal domain of the regional model are plotted in Figure 2.

The predictions of winter stratospheric temperature are consistent with the adjusted stratospheric initials – strong upper-stratospheric warming and mid and lower stratospheric cooling are obtained (Figure 2a). A slight drop of temperature is observed in the lower troposphere at high latitudes (45°–50°N). In summer, the predicted stratospheric temperature distribution is different from the initials (Figure 2b). The predicted upper and mid stratospheric temperature show a weak wave form while warmer temperatures are predicted at lower stratospheric at low latitudes and at tropopause at high latitudes. Cooling effect is basically observed in the troposphere. The temperature changes are thought to be related to the changes in solar radiation and vertical motion of atmosphere. As shown in Figure 2c,d, the SW decreased much more in summer than that in winter due to the solar zenith angle difference. The domain averaged differences of SW radiation that reached the ground in winter and summer are −0.02 and −8.7 W m2 (~3% reduction), respectively. In winter, the relatively small changes in SW radiation (less water vapor) are responsible for the small changes in the troposphere [44]. In summer, adjusted upper stratospheric temperature between 35° and 40°N shown in Figure 1b may be related to more SW absorption by the upper stratospheric ozone layer, which leads to overall decrease of SW radiation to the lower levels. The overall decrease of SW radiation then further lead to overall cooling effects in the troposphere.

The temperature difference patterns also show response to the GPH fields. In both winter and summer seasons (Figure 2e,f), the regions with decreased GPH (downward air motion) are related to those decreased temperature. GPH magnitude changes in troposphere in summer are also stronger than that in winter. The locations of the major downward atmospheric motion vary seasonallyare different in different seasons. In winter, a downward transfer of the stratospheric signal can be observed which reaches the lower troposphere between 45° and 50°N, where the FC and PC ascending part located, with a drop of GPH of less than 5 m. In contrast, the major stratospheric signal that reaches the lower troposphere is at lower latitudes (south of 35°N), where the HC descending part locate, with a drop of 3 to 6 m in summer. Tropospheric RH also shows response to the stratospheric initial conditions. Larger magnitude of RH response is also observed in summer. The strongest responses of RH are observed over the tropopause layers between 300 and 80 mb in both winter and summer. Changes of water vapor are important to the radiation balance in the tropopause layers [22]. Discontinuous radiance differences are observed in summer at 300 mb between 35° and 50°N (Figure 2d) due to enhanced water

vapor absorption over that layer (Figure 2h). But this phenomenon is not well observed in winter because the much smaller differences in SW radiation. The reasons for tropospheric RH changes are comprehensive. The factors that may affect the tropospheric RH changes may include temperature, vertical air motion, and regional atmospheric circulations.
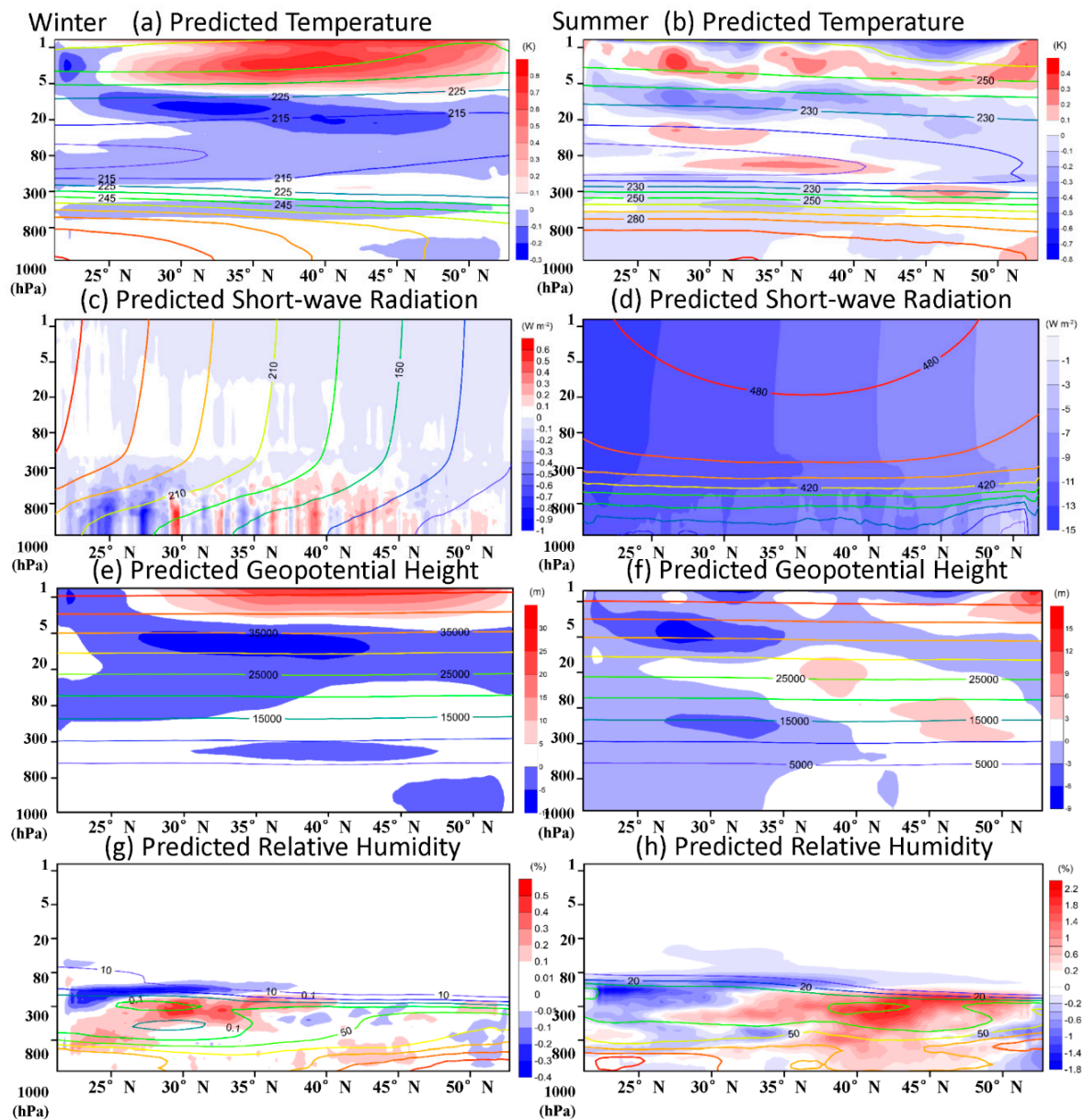

Figure 2. Zonally averaged predicted temperature (**a**,**b**), downward short-wave (SW) radiation (**c**,**d**), (GPH) (**e**,**f**), and relative humidity (RH) (**g**,**h**) differences (shaded) between EXP1 and EXP2 at the 12-h forecast lead time over the longitudinal domain of the regional model during both winter and summer and the base state (contours).

6. Responses in Medium-Range Predictions

The domain averaged vertical profiles of predicted SW radiation, temperature, GPH, and RH as a function of forecast lead times are plotted in Figure 3 using the every 12-h outputs. Turbulence of downward short-wave radiance can be observed after 48-h forecast in both winter and summer. Downward short-wave radiance is generally decreased in summer. However, the decrease and increase of downward short-wave radiance are equally distributed in winter but with smaller magnitude

than that in summer. This is strongly related to the solar zenith angle differences and the warm pool in the stratospheric initials. Relatively weak downward propagation signals are observed in winter temperature, GPH, and RH forecasts. The downward propagation signals reached the lower troposphere at 48-h forecast lead time and 132-h forecast lead time shown in the temperature and GPH panels (Figure 3c,e). This downward propagation signals are only weakly related to the downward SW radiance turbulence shown in Figure 3a. In Figure 3g, dryer tropospheric RH responses are well captured due to the downward propagation signals but with a 12-h delay. In contrast, summer temperature, GPH, and RH forecasts are strongly related to the SW radiance changes. A maximum of 5.5% reduction of downward SW radiation is obtained in the predictions due to the major absorption in the upper stratosphere shown in Figure 1b. The reduced downward SW radiance shows direct influence on the predicted temperature, GPH and RH at both upper stratosphere and lower troposphere especially at 48-, 72-, 96-, 120-, and 144-h forecast lead times. The lower troposphere patterns showed consistency to the upper stratosphere. Less downward SW radiance reached the ground leads to higher temperature, upward air motion, and lower RH, and vice versa.
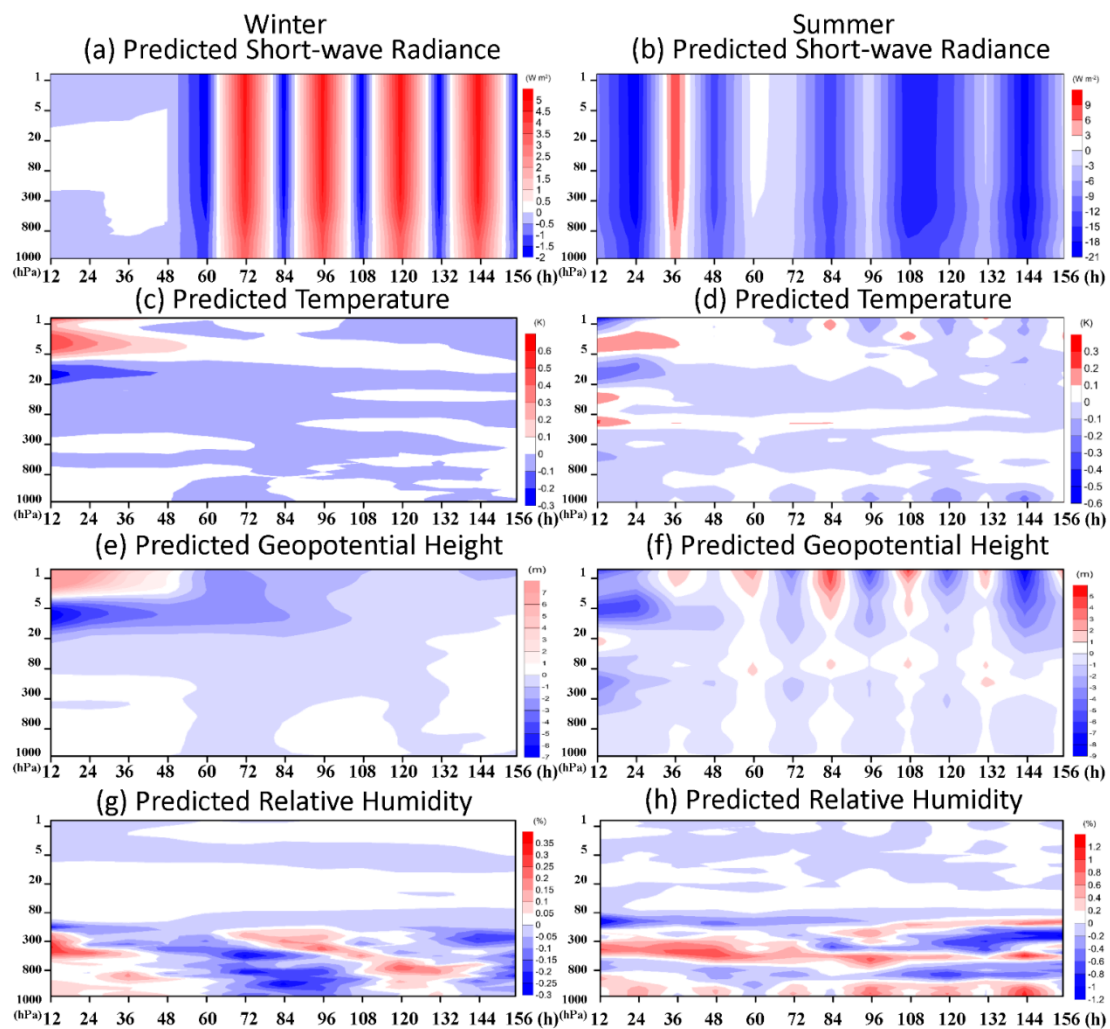

Figure 3. Domain averaged profiles of predicted downward SW radiation (**a**,**b**), temperature (**c**,**d**), GPH (**e**,**f**), and RH (**g**,**h**) differences (shaded) between EXP1 and EXP2 as a function of forecast lead times during both winter and summer.

A schematic diagram of the coupled stratosphere and troposphere is shown in Figure 4. The solar zenith angle and upper stratospheric BDC are different in winter and summer. In winter, the solar radiation is much smaller due to the fact that a much smaller zenith angle. The upper BDC descends

in the extratropical areas in winter while transporting air mass upward slightly towards north and then downward in the southern hemisphere (not plotted) in summer. The adjusted upper stratosphere initials shown in Figure 1 indicate that more absorption of SW radiance may have occurred in the upper BDC while less absorption of SW radiance in the mid and lower stratospheric BDC in both winter and summer. As a result, the reduced downward SW radiation reaching the ground lead to a change in temperature, GPH and further affect the regional atmospheric circulations and water vapor transport.
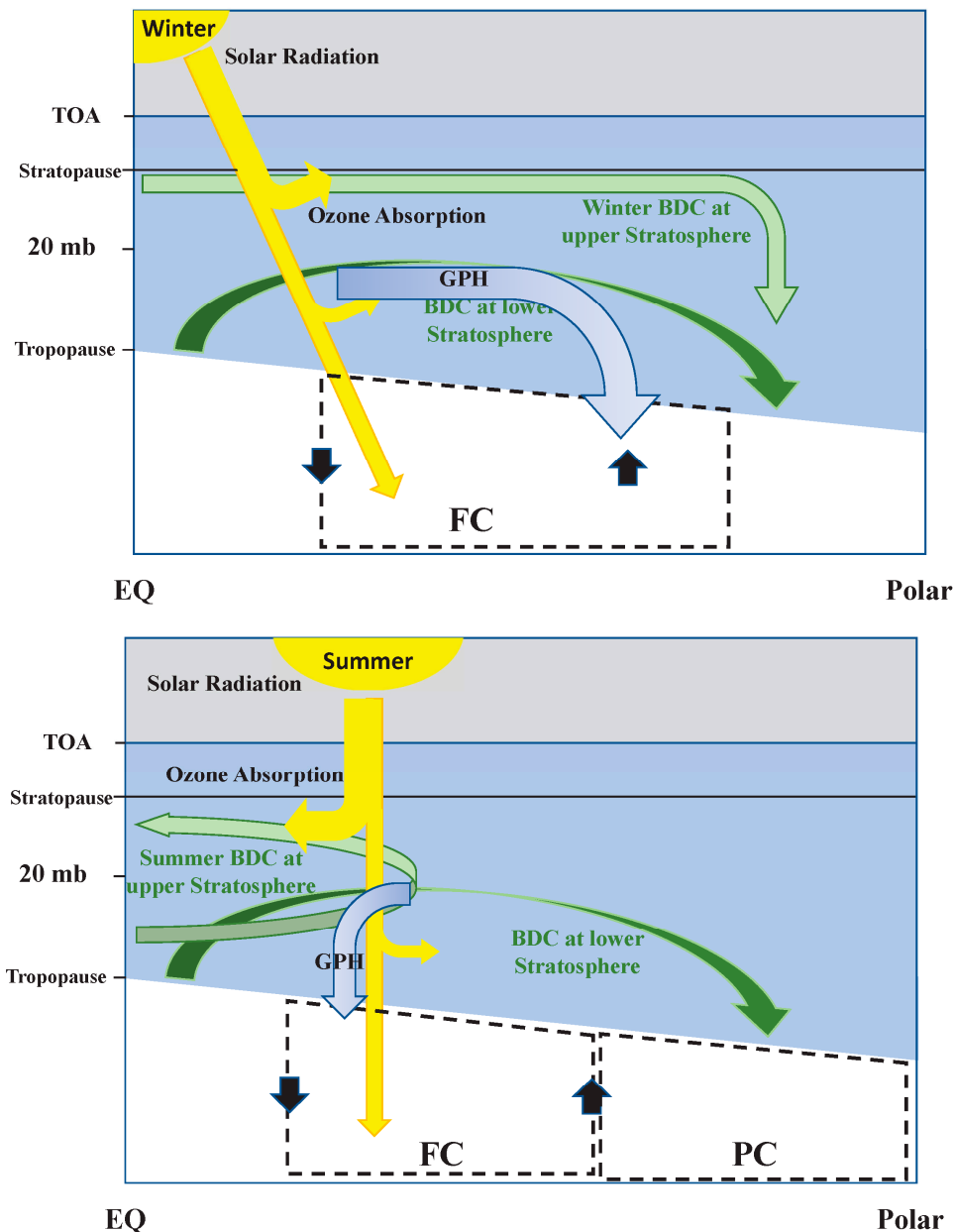
Figure 4. Schematic diagram of the fast tropospheric response to the adjusted stratospheric initials during (**a**): winter, and (**b**): summer.

7. Conclusions

This study investigated, to our knowledge for the first time, the impact of assimilated microwave stratospheric temperature measurements on a regional NWP system during a short-period forecast. A warmer upper stratosphere and cooler ozone layer are obtained in the analysis. Predicted anomalies of various variables indicate that their distributions are strongly related to the adjusted downward SW

radiation due to more absorption at upper stratosphere. However, due to the different zenith angle and intensity of solar radiation, the impacts of adjusted stratospheric initial conditions are much larger in summer those in winter. Tropospheric response in winter are relatively weak and it usually takes 48 to 72-h for the propagation of stratospheric signals to the ground. In contrast, stronger and near-instant tropospheric responses are observed in summer.

Changes in regional circulation systems due to adjusted downward SW radiation are observed in both winter and summer but with different response regions. A maximum reduction of 5.5% of downward SW radiation is obtained in the summer predictions. High latitudes are the regions showing strongest response to the stratospheric initial conditions in winter, while it is lower latitudes that show strongest response in summer. Our study results showed that the assimilated microwave temperature measurements firstly adjusted the stratospheric temperature related to upper stratospheric ozone absorption of SW radiation. A maximum of 5.5% less SW radiation reached the ground in summer leads to changes in the predicted tropospheric variables and associated regional circulation systems.

In overall, this study illustrated the importance of including the entire stratosphere in the regional NWP systems especially in summer. The 5% change in downward SW radiation and the associated changes in predictions indicates the importance of radiative processes related to ozone in the stratosphere and water vapor in the tropopause.

Conflicts of Interest: The authors declare no conflict of interest.

Abbreviations/Acronyms

WRF-ARW	Advanced Weather Research and Forecasting
Unit-A AMSU-A	Advanced Microwave Sounding
ATMS	Advanced Technology Microwave Sounder
SSMI/S	Special Sensor Microwave Imager/Sounder
GSI	Gridpoint Statistical Interpolation
SW	Short-wave
NWP	Numerical Weather Prediction
SSW	Sudden Stratospheric Warming
BDC	Brewer-Dobson Circulation
TTL	Tropical tropopause layer
NCEP	National Center for Environmental Prediction
3D-Var	Three Dimensional Variational
CRTM	Community Radiative Transfer Model
JCSDA	Joint Center for Satellite Data Assimilation
GFS	Global Forecast System
NOAA	National Oceanic and Atmospheric Administration
HC	Hadley Cell
FC	Ferrel Cell
PC	Polar Cell
GPH	Geopotential Height
RH	Relative Humidity

References

1.　Haynes, P.H.; McIntyre, M.E.; Shepherd, T.G.; Marks, C.J.; Shine, K.P. On the "Downward Control" of Extratropical Diabatic Circulations by Eddy-Induced Mean Zonal Forces. *J. Atmos. Sci.* **1991**, *48*, 651–678. [CrossRef]

2.　Norton, W.A. Tropical wave driving of the annual cycle in tropical tropopause temperatures. Part II: Model results. *J. Atmos. Sci.* **2006**, *63*, 1420–1431. [CrossRef]

3.　Sjoberg, J.P.; Birner, T. Transient Tropospheric Forcing of Sudden Stratospheric Warmings. *J. Atmos. Sci.* **2012**, *69*, 3420–3432. [CrossRef]

4.　Lu, H. Downward Wave Reflection as a Mechanism for the Stratosphere-Troposphere Response to the 11-Yr Solar Cycle. *J. Clim.* **2017**, *30*, 2395–2414. [CrossRef]

5.　Attard, H.E.; Lang, A.L. Troposphere–Stratosphere Coupling Following Tropospheric Blocking and Extratropical Cyclones. *Mon. Weather Rev.* **2019**, *147*, 1781–1804. [CrossRef]

6.　Chiba, M.; Kodera, K. Tropospheric circulation changes associated with stratospheric sudden warmings: A case study. *J. Geophys. Res. Space Phys.* **1995**, *100*, 11055.

7.　Kolstad, E.W.; Breiteig, T.; Scaife, A.A. The association between stratospheric weak polar vortex events and cold air outbreaks in the Northern Hemisphere. *Q. J. R. Meteorol. Soc.* **2010**, *136*, 886–893. [CrossRef]

8.　Lee, S.; Feldstein, S.B. Detecting Ozone- and Greenhouse Gas–Driven Wind Trends with Observational Data. *Science* **2013**, *339*, 563–567. [CrossRef]

9.　Hitchcock, P.; Simpson, I.R. The Downward Influence of Stratospheric Sudden Warmings. *J. Atmos. Sci.* **2014**, *71*, 3856–3876. [CrossRef]

10.　Yang, H. Dynamic Coupling and Chemical Transport between the Stratosphere and the Troposphere. Ph.D. Thesis, Cornell University, Ithaca, NY, USA, 2015.

11.　Kodera, K.; Mukougawa, H.; Maury, P.; Ueda, M.; Claud, C. Absorbing and reflecting sudden stratospheric warming events and their relationship with tropospheric circulation. *J. Geophys. Res. Atmos.* **2016**, *121*, 80–94. [CrossRef]

12.　Baldwin, M.P.; Dunkerton, T.J. Propagation of the Arctic Oscillation from the stratosphere to the troposphere. *J. Geophys. Res. Space Phys.* **1999**, *104*, 30937–30946. [CrossRef]

13.　Baldwin, M.P.; Dunkerton, T.J. Stratospheric Harbingers of Anomalous Weather Regimes. *Science* **2001**, *294*, 581–584. [CrossRef] [PubMed]

14.　Baldwin, M.P.; Stephenson, D.B.; Thompson, D.W.J.; Dunkerton, T.J.; Charlton, A.J.; O'Neill, A. Stratospheric memory and skill of extended-range weather forecasts. *Science* **2003**, *301*, 636–640. [CrossRef] [PubMed]

15.　Butler, A.H.; Thompson, D.W.J.; Heikes, R. The Steady-State Atmospheric Circulation Response to Climate Change–like Thermal Forcings in a Simple General Circulation Model. *J. Clim.* **2010**, *23*, 3474–3496. [CrossRef]

16.　Thomson, D.W.J.; Wallace, J.M. The Arctic Oscillation signature in the wintertime geopotential height and temperature fields. *Geophys. Res. Lett.* **1998**, *25*, 1297–1300. [CrossRef]

17.　Holton, J.R. On the Global Exchange of Mass between the Stratosphere and Troposphere. *J. Atmos. Sci.* **1989**, *47*, 392–395. [CrossRef]

18.　Butler, A.H.; Seidel, D.J.; Hardiman, S.C.; Butchart, N.; Birner, T.; Match, A. Defining sudden stratospheric warmings. *Bull. Am. Meteorol. Soc.* **2015**, *96*, 1913–1928. [CrossRef]

19.　Hegglin, M.I.; Shepherd, T.G. Large climate-induced changes in ultraviolet index and stratosphere-to-troposphere ozone flux. *Nat. Geosci.* **2009**, *2*, 687–691. [CrossRef]

20.　Charlton, J.G.; O'Neill, A.O.; Lahoz, W.A.; Massacand, A.C. Sensitivity of tropospheric forecasts to stratospheric initial conditions. *Q. J. R. Meteorol. Soc.* **2004**, *130*, 1771–1792. [CrossRef]

21.　Chiristiansen, B. Downward propagation and statistical forecast of the near-surface weather. *J. Geophys. Res.* **2005**, *110*, D14104. [CrossRef]

22.　Gettelman, A.; Forster, P.M.D.F.; Fujiwara, M.; Fu, Q.; Vömel, H.; Gohar, L.K.; Johanson, C.; Ammerman, M. Radiation balance of the tropical tropopause layer. *J. Geophys. Res. Space Phys.* **2004**, *109*, D07103. [CrossRef]

23.　Fillion, L.; Tanguay, M.; Lapalme, E.; Denis, B.; Desgagne, M.; Lee, V.; Ek, N.; Liu, Z.; Lajoie, M.; Caron, J.F.; et al. Page. The Canadian Regional Data Assimilation and Forecasting System. *Weather Forecast.* **2010**, *25*, 1645–1669. [CrossRef]

24.　Carrier, M.J.; Zou, X.; Lapenta, W.M. Comparing the Vertical Structures of Weighting Functions and Adjoint Sensitivity of Radiance and Verifying Mesoscale Forecasts Using AIRS Radiance Observations. *Mon. Weather Rev.* **2008**, *136*, 1327–1348. [CrossRef]

25. Cucurull, L.; Anthes, R.A. Impact of Infrared, Microwave, and Radio Occultation Satellite Observations on Operational Numerical Weather Prediction. *Mon. Weather Rev.* **2014**, *142*, 4164–4186. [CrossRef]

26. Zou, X.L.; Qin, Z.K.; Weng, F.Z. Improved Quantitative Precipitation Forecasts by MHS Radiance Data Assimilation with a Newly Added Cloud Detection Algorithm. *Mon. Weather Rev.* **2013**, *141*, 3203–3221. [CrossRef]

27. Shao, M. An Investigation of Multi-Satellite Stratospheric Measurements on Tropospheric Weather Predictions over Continental United States. Ph.D. Thesis, George Mason University, Fairfax, VA, USA, 2017.

28. Wang, X.G. Incorporating Ensemble Covariance in the Gridpoint Statistical Interpolation Variational Minimization: A Mathematical Framework. *Mon. Weather Rev.* **2010**, *138*, 2990–2995. [CrossRef]

29. Wang, X.; Parrish, D.; Kleist, D.; Whitaker, J. GSI 3DVar-Based Ensemble–Variational Hybrid Data Assimilation for NCEP Global Forecast System: Single-Resolution Experiments. *Mon. Weather Rev.* **2013**, *141*, 4098–4117. [CrossRef]

30. Schwartz, C.S.; Liu, Z.; Huang, X.-Y. Sensitivity of Limited-Area Hybrid Variational-Ensemble Analyses and Forecasts to Ensemble Perturbation Resolution. *Mon. Weather Rev.* **2015**, *143*, 3454–3477. [CrossRef]

31. Kleist, D.T.; Parrish, D.F.; Derber, J.C.; Treadon, R.; Wu, W.-S.; Lord, S. Introduction of the GSI into the NCEP Global Data Assimilation System. *Weather Forecast.* **2009**, *24*, 1691–1705. [CrossRef]

32. Anderson, E.; Jarvinen, H. Variational Quality Control. *Q. J. R. Meteorol. Soc.* **1998**, *125*, 697–722. [CrossRef]

33. Boukabara, S.A.; Zhu, T.; Tolman, H.L.; Lord, S.; Goodman, S.; Atlas, R.; Goldberg, M.; Auligne, T.; Pierce, B.; Cucurull, L.; et al. S4: An O2R/R2O Infrastructure for Optimizing Satellite Data Utilization in NOAA Numerical Modeling Systems: A Step Toward Bridging the Gap between Research and Operations. *Bull. Am. Meteorol. Soc.* **2016**, *97*, 2360–2378. [CrossRef]

34. Thompson, G.; Field, P.R.; Rasmussen, R.M.; Hall, W.D. Explicit Forecasts of Winter Precipitation Using an Improved Bulk Microphysics Scheme. Part II: Implementation of a New Snow Parameterization. *Mon. Weather Rev.* **2008**, *136*, 5095–5115. [CrossRef]

35. Iacono, M.J.; Delamere, J.S.; Mlawer, E.J.; Shephard, M.W.; Clough, S.A.; Collins, W.D. Radiative forcing by long-lived greenhouse gases: Calculations with the AER radiative transfer models. *J. Geophys. Res. Space Phys.* **2008**, *113*, 13103. [CrossRef]

36. Nakanishi, M.; Niino, H. Development of an Improved Turbulence Closure Model for the Atmospheric Boundary Layer. *J. Meteorol. Soc. Jpn.* **2009**, *87*, 895–912. [CrossRef]

37. Smirnova, T.G.; Brown, J.M.; Benjamin, S.G.; Kenyon, J.S. Modifications to the Rapid Update Cycle Land Surface Model (RUC LSM) available in the Weather Research and Forecast (WRF) model. *Mon. Weather Rev.* **2016**, *144*, 1851–1865. [CrossRef]

38. Grell, G.A.; Freitas, S.R. A scale and aerosol aware stochastic convective parameterization for weather and air quality modeling. *Atmos. Chem. Phys. Discuss.* **2014**, *14*, 5233–5250. [CrossRef]

39. Wu, W.-S.; Purser, R.J.; Parrish, D.F. Three-Dimensional Variational Analysis with Spatially Inhomogeneous Covariances. *Mon. Weather Rev.* **2002**, *130*, 2905–2916. [CrossRef]

40. Wang, X.G. Application of the WRF Hybrid ETKF-3DVAR Data Assimilation System for Hurricane Track Forecasts. *Mon. Weather Rev.* **2011**, *26*, 868–884. [CrossRef]

41. Benjamin, S.G.; Weygandt, S.S.; Brown, J.M.; Hu, M.; Alexander, C.R.; Smirnova, T.G.; Olson, J.B.; James, E.P.; Dowell, D.C.; Grell, G.A.; et al. A North American Hourly Assimilation and Model Forecast Cycle: The Rapid Refresh. *Mon. Weather Rev.* **2016**, *144*, 1669–1694. [CrossRef]

42. Gerber, E.P.; Orbe, C.; Polvani, L.M. Stratospheric influence on the tropospheric circulation revealed by idealized ensemble forecasts. *Geophys. Res. Lett.* **2009**, *36*, 24801. [CrossRef]

43. Karpechko, A.Y.; Hitchcock, P.; Peters, D.H.W.; Schneidereit, A. Predictability of downward propagation of major sudden stratospheric warmings. *Q. J. R. Meteorol. Soc.* **2017**, *143*, 1459–1470. [CrossRef]

44. Gilford, D.M.; Solomon, S. Radiative Effects of Stratospheric Seasonal Cycles in the Tropical Upper Troposphere and Lower Stratosphere. *J. Clim.* **2017**, *30*, 2769–2783. [CrossRef]